



HAL
open science

VLBA Reveals the Absence of a Compact Radio Core in the Radio-intermediate Quasar J2242+0334 at $z = 5.9$

Yuanqi Liu, Ran Wang, Emmanuel Momjian, Yingkang Zhang, Tao An, Xiaolong Yang, Jeff Wagg, Eduardo Bañados, Alain Omont

► **To cite this version:**

Yuanqi Liu, Ran Wang, Emmanuel Momjian, Yingkang Zhang, Tao An, et al.. VLBA Reveals the Absence of a Compact Radio Core in the Radio-intermediate Quasar J2242+0334 at $z = 5.9$. The Astrophysical journal letters, 2022, 939, 10.3847/2041-8213/ac98b2 . insu-03839626

HAL Id: insu-03839626

<https://insu.hal.science/insu-03839626>

Submitted on 4 Nov 2022

HAL is a multi-disciplinary open access archive for the deposit and dissemination of scientific research documents, whether they are published or not. The documents may come from teaching and research institutions in France or abroad, or from public or private research centers.

L'archive ouverte pluridisciplinaire **HAL**, est destinée au dépôt et à la diffusion de documents scientifiques de niveau recherche, publiés ou non, émanant des établissements d'enseignement et de recherche français ou étrangers, des laboratoires publics ou privés.



Distributed under a Creative Commons Attribution 4.0 International License



VLBA Reveals the Absence of a Compact Radio Core in the Radio-intermediate Quasar J2242+0334 at $z = 5.9$

Yuanqi Liu^{1,2} , Ran Wang² , Emmanuel Momjian³ , Yingkang Zhang¹ , Tao An¹ , Xiaolong Yang¹ , Jeff Wagg⁴,
Eduardo Bañados⁵ , and Alain Omont⁶ 

¹ Shanghai Astronomical Observatory, Key Laboratory of Radio Astronomy, CAS, 80 Nandan Road, Shanghai 200030, People's Republic of China

² Department of Astronomy, Peking University, Beijing 100871, People's Republic of China; rwangkiaa@pku.edu.cn

³ National Radio Astronomy Observatory, P.O. Box O, Socorro, NM 87801, USA

⁴ SKA Observatory, Lower Withington Macclesfield, Cheshire SK11 9FT, UK

⁵ Max-Planck-Institut für Astronomie, Königstuhl 17, D-69117 Heidelberg, Germany

⁶ Institut d'Astrophysique de Paris, Sorbonne Université, CNRS, UMR 7095, 98 bis bd Arago, F-75014 Paris, France

Received 2022 August 28; revised 2022 September 28; accepted 2022 October 5; published 2022 October 26

Abstract

High-resolution imaging is crucial for exploring the origin and mechanism of radio emission in quasars, especially at high redshifts. We present 1.5 GHz Very Long Baseline Array (VLBA) images of the radio continuum emission from the radio-intermediate quasar (RIQ) J2242+0334 at $z = 5.9$. This object was previously detected at both 1.5 GHz and 3 GHz with the Karl G. Jansky Very Large Array (VLA) as a point source. However, there is no clear detection in the VLBA images at both the full resolution of $10.7 \text{ mas} \times 4.5 \text{ mas}$ ($61.7 \text{ pc} \times 26.0 \text{ pc}$) and a tapered resolution of $26 \text{ mas} \times 21 \text{ mas}$ ($150 \text{ pc} \times 121 \text{ pc}$). This suggests that the radio emission from the quasar is diffuse on milliarcsecond scales with surface brightness fainter than the 3σ detection limit of $40.5 \mu\text{Jy beam}^{-1}$ in the full-resolution image. The radio emission in the RIQ J2242+0334 is likely to be wind-like (i.e., diffuse) rather than in the form of collimated jets. This is different from the previous radio detections of the most luminous quasars at $z \sim 6$ that are usually dominated by compact, high brightness temperature radio sources. Meanwhile, compared with RIQs at low redshifts, the case of J2242+0334 suggests that not all RIQs are beamed radio-quiet quasars. This optically faint RIQ provides an important and unique example to investigate the radio activity in the less powerful active galactic nuclei at the earliest cosmic epoch.

Unified Astronomy Thesaurus concepts: Radio continuum emission (1340); Early universe (435); Quasars (1319)

1. Introduction

High-redshift quasars are ideal targets to explore the rapid accretion of supermassive black holes (SMBHs) and the nuclear activity at an early evolutionary stage (Volonteri 2012; Shen et al. 2019). Currently, more than 300 quasars have been discovered at redshift $z \geq 5.7$, within the first 1 Gyr after the Big Bang (e.g., Fan et al. 2000, 2001; Willott et al. 2010a, 2010b; Banados et al. 2016; Jiang et al. 2016; Matsuoka et al. 2016, 2018a; Wang et al. 2019). The radio-loud fraction is constrained to be 10% among these quasars (Banados et al. 2018; Liu et al. 2021). Previously, eight radio sources at $z \sim 6$ were imaged using Very Long Baseline Interferometry (VLBI) on scales of a few tens of parsecs to kiloparsec (e.g., Frey et al. 2011; Cao et al. 2014; Momjian et al. 2018, 2021; Zhang et al. 2021). The VLBI images of these high- z quasars reveal compact radio cores and/or ~ 1 kpc scale radio jets, which are similar to the compact/medium-size symmetric objects (CSOs/MSOs) found at lower redshift (Taylor et al. 2000; Conway 2002; An & Baan 2012), arguing for a young radio-loud AGN at its early evolutionary stage.

These existing VLBI observations mainly focus on the most radio powerful objects at $z \sim 6$ with radio-loudness $R > 100$ ($R = f_{\text{radio}}/f_{\text{optical}}$), e.g., P352-15 with $R > 1000$ (Banados et al. 2018; Momjian et al. 2018), and blazar PSO J0309+27 with $R = 2500 \pm 500$ at $z \geq 6$ (Belladitta et al. 2020; Spingola et al. 2020). Although it is limited by the sensitivity of the telescopes,

studying much weaker sources is crucial to understanding the radio properties of the whole quasar population in the distant universe.

In this Letter, we present Very Long Baseline Array (VLBA) observations of a less luminous radio quasar CFHQS J224237+033421 (hereafter J2242+0334) at redshift 5.9, which is discovered in the Canada-France High- z Quasar Survey (CFHQS; Willott et al. 2010a). This quasar has a bolometric luminosity of $L_{\text{bol}} = 4.2 \times 10^{12} L_{\odot}$, converted from the absolute magnitude of -24.17 at rest-frame 1450 \AA (Willott et al. 2010a; Liu et al. 2021). It is at the faint end of the quasar luminosity function that spans a range from 10^{11} to $10^{14} L_{\odot}$ (Wu et al. 2015; Matsuoka et al. 2018b; Shen et al. 2019). As indicated by the quasar luminosity function, the relatively optically faint quasars at $z \sim 6$ discovered from the deep optical and near-infrared surveys represent the more common quasar population in the early universe (Matsuoka et al. 2018b).

Subsequent radio observation of J2242+0334 using the Karl G. Jansky Very Large Array (VLA) measures the radio-loudness of $R = f_{5 \text{ GHz}}/f_{4400 \text{ \AA}} = 54.9 \pm 4.7$ (Kellermann et al. 1989; Liu et al. 2021). This value is above the boundary of $R = 10$ for radio-loud quasars (Kellermann et al. 1989). In contrast to the bright radio sources with $R > 100$, such objects with a less powerful radio source are usually called radio-intermediate quasars (RIQs, i.e., $3 < R < 100$) in the literature (Miller et al. 1993; Diamond-Stanic et al. 2009; Goyal et al. 2010). Thus, J2242+0334 provides us a unique opportunity to investigate the early radio activity of radio-intermediate quasars.

J2242+0334 has been observed by VLA at both 3 GHz and 1.4 GHz (Liu et al. 2021). The VLA observation of J2242+0334 at 3 GHz and spatial resolution of $0''.8 \times 0''.7$

(4.6 kpc \times 4.0 kpc) revealed an unresolved radio source with a flux density $S_{\text{VLA-3GHz}} = 87.0 \pm 6.3 \mu\text{Jy}$ at the optical quasar position. Observations at 1.4 GHz also reported an unresolved source with a flux density $S_{\text{VLA-1.4GHz}} = 195.9 \pm 24.7 \mu\text{Jy}$ and a restoring beam size of $1''.4 \times 1''.2$ (8.0 kpc \times 6.9 kpc). Here, we present the VLBA observation of this object at 1.5 GHz with milliarcsecond resolution to further investigate the nature of the radio emission. The observations and data reduction are described in Section 2. We present the results in Section 3, and the discussion in Section 4. Section 5 summarizes the conclusions.

Throughout this work, we adopt a Λ CDM cosmology with $H_0 = 70 \text{ km s}^{-1} \text{ Mpc}^{-1}$, $\Omega_m = 0.3$, and $\Omega_\Lambda = 0.7$. With this cosmological model, $1''$ at the redshift of J2242+0334 corresponds to 5.77 kpc.

2. Observation and Data Reduction

The VLBA observations (project code: BL280) of the quasar J2242+0334 were conducted at 1.5 GHz (L band, 20 cm) during 2020 October 16–18. The observations were divided into three separate observing sessions. The optical coordinates (J2000) of the quasar are R.A. = $22^{\text{h}}42^{\text{m}}37^{\text{s}}.533$, decl. = $+03^{\circ}34'22''.03$. The radio center coordinates in VLA 3 GHz images are R.A. = $22^{\text{h}}42^{\text{m}}37^{\text{s}}.5306$, decl. = $+03^{\circ}34'22''.0445$, which are used as the target phase center in VLBA observations. All 10 VLBA stations were used. The total bandwidth, from 1.35 to 1.75 GHz, was composed of eight discrete 32 MHz intermediate frequency channels (IFs) in both right- and left-hand circular polarizations. Each channel was further split into 256 spectral points. The spectral points affected by radio frequency interference (RFI) were flagged before calibration. The data were recorded at each station with the ROACH Digital Backend and the polyphase filterbank (PFB) digital signal-processing algorithm with a data rate of 2048 Mbps. Then, the data were correlated with 2 s correlator integration time, using the VLBA DiFX correlator in Socorro, NM.

For the target, we employed a nodding-style phase-referencing observing strategy with a series of 4 minute cycles, comprising 3 minutes on the target and 1 minute on the phase calibrator. The total observing time was 12 hr, with 8.4 hr on target. We chose a bright and nearby phase calibrator J2245+0500 ($S_{1.5 \text{ GHz}} = 153.3 \pm 1.2 \text{ mJy}$), which was $1''.7$ away from the target. The source 3C454.3 was used as the fringe finder and bandpass calibrator.

The data were edited and calibrated using the US National Radio Astronomy Observatory (NRAO) Astronomical Image Processing System (AIPS; Greisen 2003) in a standard way. Imaging and the CLEAN task of the target and calibrators were applied with the Caltech Difmap (Shepherd 1997). Then we performed self-calibration for both phase and amplitude on the phase calibrator J2245+0500 based on its CLEAN model. The self-calibration resolutions were also applied to the target visibility data. The main parameters of the VLBA observations are summarized in Table 1.

3. Results and Analysis

We first image the VLBA data at its full resolution and natural weighting. The FWHM beam size is $10.7 \times 4.5 \text{ mas}$ (61.7 pc \times 26.0 pc at $z = 5.9$) and the 1σ rms is $13.5 \mu\text{Jy beam}^{-1}$ (Figure 1). No radio source is detected at the optical quasar or VLA radio source position, which are $0''.4$ apart. This

Table 1
Observation Parameters

Observing central frequency (GHz)	1.5
Recorded bandwidth (MHz)	256
Date of observations (in 2020)	Oct 16–18
Phase calibrator	J2245+0500
Flux/Bandpass calibrator	3C454.3
Full-resolution image:	
FWHM beam size ^a (mas)	10.7×4.5
Beam P.A. ($^\circ$)	-2.8
Image 1σ rms sensitivity ($\mu\text{Jy beam}^{-1}$)	13.5
Brightness temperature (K)	$\leq 3 \times 10^6$
Tapered image at $4M\lambda$:	
FWHM beam size ^a (mas)	26×21
Beam P.A. ($^\circ$)	22.0
Image 1σ rms sensitivity ($\mu\text{Jy beam}^{-1}$)	32.6

Note.

^a Natural weighting.

results in a 3σ upper limit of $40.5 \mu\text{Jy beam}^{-1}$ for the surface brightness of the radio source. This estimates the intrinsic brightness temperature to be $T_b \leq 3 \times 10^6 \text{ K}$ for any compact radio source at the quasar position. Here we estimate the 3σ upper limit of the intrinsic brightness temperature adopting the equation in Taylor et al. (1999):

$$T_b = 1.22 \times 10^{12} (1+z) \frac{S_\nu}{\nu^2 \theta_{\text{max}} \theta_{\text{min}}}, \quad (1)$$

where ν is the observing frequency in GHz, S_ν is the surface brightness detection limit in Jy beam^{-1} , and the resolution $\theta_{\text{max}} = 10.7 \text{ mas}$ and $\theta_{\text{min}} = 4.5 \text{ mas}$, which is converted from the Rayleigh–Jeans law ($T_b = \frac{\chi^2}{2k\Omega} S$, k is the Boltzmann constant and Ω is the beam solid angle).

To reduce the resolution and recover more extended emission, we apply a two-dimensional Gaussian taper to the UV visibility data, which reduces the weight to 50% at UV distance $4M\lambda$ (in units of wavelength). The resolution of the tapered image is $26 \text{ mas} \times 21 \text{ mas}$ (150 pc \times 121 pc). No $> 5\sigma$ signal is detected in the source radio position and surrounding 5 kpc area.

4. Discussions

The nondetection of J2242+0334 in the VLBA image, together with the previous VLA detection, constrains the spatial extent of the radio emission from this object. The source is unresolved with the VLA in B-array configuration (Liu et al. 2021) with a minimum resolvable size to be $\theta = b \sqrt{\frac{4 \ln 2}{\pi} \ln \left(\frac{\text{SNR}}{\text{SNR} - 1} \right)} = 0''.4$, where $b = \sqrt{b_{\text{max}} \times b_{\text{min}}} = 1''.3$ is the beam size (Kovalev et al. 2005). This minimum resolvable size corresponds to 2.3 kpc at the redshift of J2242+0334. The nondetection in both the full-resolution and the tapered VLBA images suggest that the emission detected by the VLA is not from a compact source at the milliarcsecond-scale resolution. The radio emission is diffuse on tens of milliarcseconds to subarcsecond (tens of parsecs to kiloparsec) scales.

The 1.4 GHz and 3 GHz data presented in Liu et al. (2021) show a steep power-law spectrum with a spectral index $\alpha_R = -1.07_{-0.25}^{+0.27}$ (adopting the model $S_\nu \propto \nu^\alpha$). This steep spectrum indicates that the diffuse radio emission detected in

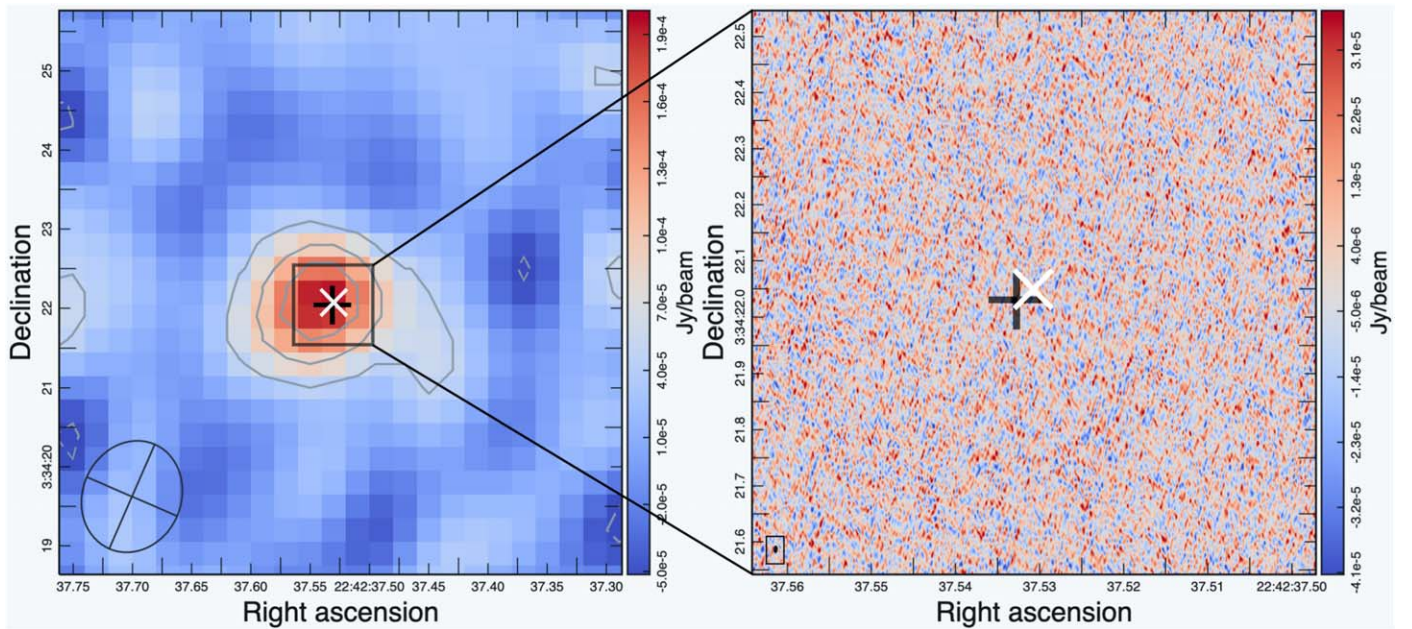


Figure 1. Left panel: the intensity map of VLA observations at 1.4 GHz. The contour levels are at $[-1, 2, 4, 6]$ times the corresponding 1σ rms noise level of $24.7\ \mu\text{Jy beam}^{-1}$. The synthesized beam with an FWHM of $1''.4 \times 1''.2$ is shown as an ellipse in the bottom left corner. Right panel: full-resolution VLBA image in $1'' \times 1''$ area, zooming into the central area in the VLA image. A synthesized beam with an FWHM of $10.7\ \text{mas} \times 4.5\ \text{mas}$ is shown as the ellipse in the bottom left black square box. For both panels, the black plus denotes the optical position and the white cross represents the peak position in VLA 3 GHz observations (Liu et al. 2021), which is also the phase center of the VLBA observations.

J2242+0334 is likely to be dominated by optically thin synchrotron emission (O’Dea & Saikia 2021; Silpa et al. 2021; Patil et al. 2022). Such optically thin synchrotron emission with resolved/extended morphology and steep spectra was typical for radio-quiet quasars observed at low redshifts (e.g., Pei et al. 2020).

The radio emission, although diffuse, is unlikely to be powered primarily by nuclear star formation. If the VLA-detected radio emission $S_{\text{VLA-1.4GHz}} = 195.9 \pm 24.7\ \mu\text{Jy}$ is all from star formation, the star formation rate (SFR) would be $\sim 55,000\ M_{\odot}\ \text{yr}^{-1}$, according to the relation in Murphy et al. (2011):

$$\left(\frac{\text{SFR}_{1.4\text{GHz}}}{M_{\odot}\ \text{yr}^{-1}}\right) = 6.35 \times 10^{-29} \left(\frac{L_{1.4\text{GHz}}}{\text{erg s}^{-1}\text{Hz}^{-1}}\right), \quad (2)$$

where the rest-frame radio luminosity at 1.4 GHz is extrapolated with the spectral index measured by VLA. However, J2242+0334 was not detected by Herschel in bright dust continuum in submillimeter Bands. Lyu et al. (2016) constrained the SFR upper limit of J2242+0334 to be $< 2561\ M_{\odot}\ \text{yr}^{-1}$ from the integrated infrared (IR) luminosity upper limit. The difference between SFRs converted from radio and the IR detection limit suggests that star formation cannot be the dominant power source of the detected radio emission with the VLA. Thus, most of the radio emission from J2242+0334 is likely to be powered by the AGN. One possibility is that the VLA-detected radio flux density consists of winds or several knots with surface brightness below the detection limit. Furthermore, a less powerful jet may interact with the surrounding medium, which could also result in extended radio emission. Such systems were identified in some local quasars with radio and X-ray observations (Wills et al. 1999; Kunert-Bajraszewska et al. 2010; Silpa et al. 2021).

4.1. Comparison with Quasars at $z \sim 6$

Currently, among more than 300 quasars found at $z > 5.7$, only 8 (7 radio-loud and 1 radio-quiet) quasars have been observed with the VLBI technique before this work. Among these, J2242+0334 is the first source that no compact core is detected at milliarcsecond-scale resolution, despite being comparable or even deeper VLBI observations.

All the previous seven radio-loud quasars are observed in the form of compact structures at the milliarcsecond scale, showing as a radio core (e.g., P172+18, Momjian et al. 2021; J2318-3113, Zhang et al. 2021) or multiple components (one-sided jet or CSOs, e.g., J1427+3312, Frey et al. 2008; PSO J352.4034-15.3373, Momjian et al. 2018). They are reported with high intrinsic brightness temperatures of 10^6 – $10^9\ \text{K}$ and relatively steep spectra ($\alpha = -1.1 \sim -0.8$). These radio-loud sources appear to be the early stage of powerful radio galaxies.

Comparing the VLA and VLBI observations at the same frequency, at least two quasars (SDSS J2228+0110, Cao et al. 2014; PSO J352.4034-15.3373, Momjian et al. 2018) report significant flux density differences ($> 50\%$). The differences between VLA and VLBA for these two objects indicate the radio emission from both compact core and extended component (likely to be winds) on kiloparsec scales. Compared to these radio-loud quasars, J2242+0334 seems to be dominated by diffuse, large-scale emission along with likely small-scale emission too faint to be detected in our observations.

The only radio-quiet ($R = 0.6$) quasar at $z > 6$ with VLBI observations so far, J0100+2802, shows an unresolved radio core ($88 \pm 19\ \mu\text{Jy}$) in the VLBA image at $\sim 10\ \text{mas}$ resolution (Wang et al. 2017). The compact core accounts for about 65% of the flux density detected by the VLA at the same frequency ($136.2 \pm 10.4\ \mu\text{Jy}$) observed in the same year (Liu et al. 2022). J2242+0334 and J0100+2802 have a comparable radio flux density in the VLA observations (Wang et al. 2016). However,

they are quite different on milliarcsecond scales as J2242+0334 shows no compact radio source, while J0100+2802 shows a compact source with high brightness temperature $T_b = (1.6 \pm 1.2) \times 10^7$ K and a relatively flat spectrum with the power-law index of $\alpha = -0.52 \pm 0.18$ fitted from VLA observations at 1.5 GHz, 6 GHz, and 10 GHz.

Compared to J0100+2802 with a bolometric luminosity of $L_{\text{bol}} = 4.29 \times 10^{14} L_{\odot}$ (Wu et al. 2015), which hosts the most massive and luminous AGN, the nucleus of J2242+0334 is much less powerful with a bolometric luminosity about 2 orders of magnitude smaller. Although there is radio activity from both nuclei with comparable radio flux density, the jet from J2242+0334 may be less energetic and/or uncollimated. Such an uncollimated jet or wind-like structure may interact with the surrounding medium with a large impact factor, resulting in diffuse radio emission.

4.2. Comparison with Low-redshift RIQs

The RIQ population at low redshifts were observed and studied at both VLA and VLBI scale, to explore the nature of their radio activity and to understand how they compare to the radio-quiet and radio-loud objects. A substantial fraction of RIQs is suggested to be relativistically beamed counterparts of weak jets in radio-quiet quasars, based on their observational features of core-dominated morphology (a few have extended emissions) with flat radio spectra and optical variability (Falcke et al. 1996; Wang et al. 2006; Goyal et al. 2010). However, the beaming scenario is not conclusive from the study of 11 RIQs at redshift 2–4 with the European Very-Long-Baseline-Interferometry Network (EVN) observations (Klockner et al. 2009). Among the sample of 11 RIQs, compact cores are detected in seven sources while $\sim 40\%$ of the VLA measured flux densities are resolved out on a scale larger than 150 pc. Therefore, not all of these quasars can be explained as beamed radio-quiet quasars. The fraction of the emission resolved out by EVN can be related to the size and orientation of the jet. In the case of J2242+0334, the radio emission is totally resolved out in the VLBA image. Therefore, it is unlikely to be a beamed source.

The best-studied RIQ, III Zw 2, is highly variable, containing complex components at kpc scales, including jets, lobes and uncollimated winds (Brunthaler et al. 2000, 2005). The polarization study indicates that the weak jet in this RIQ is suppressed by the surrounding strong wind-like component. Radio variability and polarization structures also indicate that the jet activity is intermittent, which may be explained by changing spectral states of the accretion disk in an ongoing merger event (Silpa et al. 2021). Our VLBA observation of J2242+0334 reveals similar radio emission properties with III Zw 2, where the diffuse emission is the dominant component for the emission detected with the VLA. It is possible that J2242+0334 is the counterpart of the RIQ systems like III Zw 2 at the highest redshift. Further monitoring of the radio variability and accurate measurements of the black hole mass and X-ray luminosity will help to explore the evolutionary properties of the central engine, e.g., intermittent activity, changes of accretion disk states, and surrounding magnetic field influence.

5. Summary

We carried out VLBA observations on the radio-intermediate quasar J2242+0334 at $z = 5.9$. The source is undetected in both full-resolution and tapered images. We provide here a point-source 3σ detection limit of $40.5 \mu\text{Jy beam}^{-1}$ at $10.7 \text{ mas} \times 4.5 \text{ mas}$ resolution. The brightness temperature is constrained to be $T_b \leq 3 \times 10^6$ K. This is the first time we report diffuse radio emission from an RIQ at $z \sim 6$, which is fully resolved out at the resolution of VLBA. Such extended radio emission with low surface brightness is likely dominated by weak (undetected) jet knots and/or originates from the interaction between the weak jet and the surrounding medium. It also indicates that not all RIQs are beamed radio-quiet quasars. Thus, J2242+0334 makes a unique example for the complex radio activity in the RIQ in the early universe.

We acknowledge support from the National Science Foundation of China (NSFC) grants Nos. 11991052, 11721303, 12173002, 11373008, 11533001. Y.K.Z. was sponsored by the Shanghai Sailing Program under grant No. 22YF1456100. The National Radio Astronomy Observatory (NRAO) is a facility of the National Science Foundation operated under cooperative agreement by Associated Universities, Inc. This Letter makes use of the VLBA data from program BL280.

Facilities: VLBA, AIPS, Difmap.

ORCID iDs

Yuanqi Liu  <https://orcid.org/0000-0001-9321-6000>
 Ran Wang  <https://orcid.org/0000-0003-4956-5742>
 Emmanuel Momjian  <https://orcid.org/0000-0003-3168-5922>
 Yingkang Zhang  <https://orcid.org/0000-0001-8256-8887>
 Tao An  <https://orcid.org/0000-0003-4341-0029>
 Xiaolong Yang  <https://orcid.org/0000-0001-5323-0764>
 Eduardo Bañados  <https://orcid.org/0000-0002-2931-7824>
 Alain Omont  <https://orcid.org/0000-0002-4721-3922>

References

- An, T., & Baan, W. A. 2012, *ApJ*, 760, 77
 Banados, E., Carilli, C., Walter, F., et al. 2018, *ApJL*, 861, L14
 Banados, E., Venemans, B. P., Decarli, R., et al. 2016, *ApJS*, 227, 11
 Belladitta, S., Moretti, A., Caccianiga, A., et al. 2020, *A&A*, 635, L7
 Brunthaler, A., Falcke, H., Bower, G. C., et al. 2000, *A&A*, 357, L45
 Brunthaler, A., Falcke, H., Bower, G. C., et al. 2005, *A&A*, 435, 497
 Cao, H.-M., Frey, S., Gurvits, L. I., et al. 2014, *A&A*, 563, A111
 Conway, J. E. 2002, *NewAR*, 46, 263
 Diamond-Stanic, A. M., Fan, X., Brandt, W. N., et al. 2009, *ApJ*, 699, 782
 Falcke, H., Patnaik, A. R., & Sherwood, W. 1996, *ApJL*, 473, L13
 Fan, X., Narayanan, V. K., Lupton, R. H., et al. 2001, *AJ*, 122, 2833
 Fan, X., White, R. L., Davis, M., et al. 2000, *AJ*, 120, 1167
 Frey, S., Gurvits, L. I., Paragi, Z., & Gabanyi, K. E. 2008, *A&A*, 484, L39
 Frey, S., Paragi, Z., Gurvits, L. I., Gabanyi, K. E., & Cseh, D. 2011, *A&A*, 531, L5
 Goyal, A., Gopal-Krishna, J. S., et al. 2010, *MNRAS*, 401, 2622
 Greisen, E. W. 2003, in *Information Handling in Astronomy—Historical Vistas*, Astrophysics and Space Science Library, Vol. 285, ed. A. Heck (Dordrecht: Kluwer Academic), 109
 Jiang, L., McGreer, I. D., Fan, X., et al. 2016, *ApJ*, 833, 222
 Kellermann, K. I., Sramek, R., Schmidt, M., Shaffer, D. B., & Green, R. 1989, *AJ*, 98, 1195
 Klockner, H.-R., Martinez-Sansigre, A., Rawlings, S., & Garrett, M. A. 2009, *MNRAS*, 398, 176
 Kovalev, Y. Y., Kellermann, K. I., Lister, M. L., et al. 2005, *AJ*, 130, 2473

- Kunert-Bajraszewska, M., Janiuk, A., Gawronski, M. P., & Siemiginowska, A. 2010, *ApJ*, **718**, 1345
- Liu, Y., Wang, R., Momjian, E., et al. 2021, *ApJ*, **908**, 124
- Liu, Y., Wang, R., Momjian, E., et al. 2022, *ApJ*, **929**, 69
- Lyu, J., Rieke, G. H., & Alberts, S. 2016, *ApJ*, **816**, 85
- Matsuoka, Y., Iwasawa, K., Onoue, M., et al. 2018a, *ApJS*, **237**, 5
- Matsuoka, Y., Onoue, M., Kashikawa, N., et al. 2016, *ApJ*, **828**, 26
- Matsuoka, Y., Strauss, M. A., Kashikawa, N., et al. 2018b, *ApJ*, **869**, 150
- Miller, P., Rawlings, S., & Saunders, R. 1993, *MNRAS*, **263**, 425
- Momjian, E., Banados, E., Carilli, C. L., Walter, F., & Mazzucchelli, C. 2021, *AJ*, **161**, 207
- Momjian, E., Carilli, C. L., Banados, E., Walter, F., & Venemans, B. P. 2018, *ApJ*, **861**, 86
- Murphy, E. J., Condon, J. J., Schinnerer, E., et al. 2011, *ApJ*, **737**, 67
- O'Dea, C. P., & Saikia, D. J. 2021, *A&ARv*, **29**, 3
- Patil, P., Whittle, M., Nyland, K., et al. 2022, *ApJ*, **934**, 26
- Pei, Z.-Y., Fan, J.-H., Bastieri, D., et al. 2020, *RAA*, **20**, 025
- Shen, Y., Wu, J., Jiang, L., et al. 2019, *ApJ*, **873**, 35
- Shepherd, M. C. 1997, in ASP Conf. Ser. 125, *Astronomical Data Analysis Software and Systems VI*, ed. G. Hunt & H. Payne (San Francisco, CA: ASP), 77
- Silpa, S., Kharb, P., Harrison, C. M., et al. 2021, *MNRAS*, **507**, 991
- Spingola, C., Dallacasa, D., Belladitta, S., et al. 2020, *A&A*, **643**, L12
- Taylor, G. B., Carilli, C. L., & Perley, R. A. (ed.) 1999, in ASP Conf. Ser. 180, *Synthesis Imaging in Radio Astronomy II* (San Francisco, CA: ASP)
- Taylor, G. B., Marr, J. M., Pearson, T. J., & Readhead, A. C. S. 2000, *ApJ*, **541**, 112
- Volonteri, M. 2012, *Sci*, **337**, 544
- Wang, F., Yang, J., Fan, X., et al. 2019, *ApJ*, **884**, 30
- Wang, R., Momjian, E., Carilli, C. L., et al. 2017, *ApJL*, **835**, L20
- Wang, R., Wu, X.-B., Neri, R., et al. 2016, *ApJ*, **830**, 53
- Wang, T.-G., Zhou, H.-Y., Wang, J.-X., Lu, Y.-J., & Lu, Y. 2006, *ApJ*, **645**, 856
- Willott, C. J., Albert, L., Arzoumanian, D., et al. 2010b, *AJ*, **140**, 546
- Willott, C. J., Delorme, P., Reylé, C., et al. 2010a, *AJ*, **139**, 906
- Wills, B. J., Brandt, W. N., & Laor, A. 1999, *ApJL*, **520**, L91
- Wu, X.-B., Wang, F., Fan, X., et al. 2015, *Natur*, **518**, 512
- Zhang, Y., An, T., Frey, S., et al. 2021, *MNRAS*, **507**, 3736